Binder MIMO Channels

Bin Lee, John M. Cioffi, *Fellow, IEEE*, Sumanth Jagannathan, *Student Member, IEEE*, Kibeom Seong, *Student Member, IEEE*, Youngjae Kim, *Student Member, IEEE*, Mehdi Mohseni, *Student Member, IEEE*, and Mark H. Brady

***Abstract*—This paper introduces a multiple-input multiple-output channel model for the characterization of a binder of telephone lines. This model is based on multiconductor transmission line theory, and uses parameters that can be obtained from electromagnetic theory or measured data. The model generates frequency-dependent channel/binder transfer function matrices as a function of cable type, geometric line-spacing and twist-length parameters, and source–load configurations. The model allows the extraction of the magnitude and the phase of individual near end crosstalk, far end crosstalk, split-pair, and phantom transfer functions from the transfer function matrix of the binder. These individual crosstalk transfer functions are often found to be very sensitive to small imperfections in the binder. Examples of category 3 twisted pair American telephone lines and "quad" telephone cables are also presented.**

***Index Terms*—Crosstalk, multiconductor transmission lines (MTLs), multiple-input multiple-output (MIMO) systems, subscriber loops, twisted pair cables.**

I. Introduction

TWISTED pair telephone line models in use today have largely been of an individual line's insertion loss and transfer function. These models have well served the digital subscriber line (DSL) and 10/100/G Ethernet communities. However, with new vectored and/or bonded DSL systems for mitigating, and possibly, exploiting the crosstalk between multiple lines [1], [2], models for a binder of twisted pairs need significant improvement. This paper introduces a multiple-input multiple-output (MIMO) model for telephone lines that allows computation of both the magnitude and phase of all the possible energy transfer functions within a binder, be it the direct-line transfer function or the various types of crosstalks. The intent of the model is to enable more accurate and dependable characterization of the various MIMO methods that can be applied to the binders of twisted pairs to increase data rates, and in particular, to model the use of telephone lines for bandwidths of 100 s of megabits per second, or possibly, even a gigabit per second, while allowing 100 m categories 5e, 6, and 7 transmission of 10 Gbps Ethernet data rates (i.e., 10GBASE-T).

The focus of this paper will be to extend the well-known resistance–inductance–capacitance–conductance (RLCG) [3] models for individual twisted pairs to matrix RLCG models, and to obtain the necessary parameters for MIMO transmission methods. The matrix RLCG models have been examined for general electromagnetic coupling by Paul [4], while the steady-state solutions for multiterminal transmission lines were found by Rice [5]. This paper focuses on a multiple-twisted pair binder with N pairs, or equivalently, $2N$ wires. Such a binder has can be modeled by $2N-1$ voltages. When a cable has a shield, there will be $2N+1$ conductors, and the general theory presented in this paper still applies except that a different geometrical description of cable is needed [6]. This paper introduces load and source matrices, and the potential of matrix-matched load impedances, which is conceptually similar to the single-line case but greatly differs in the implementation for MIMO binders. This paper also illustrates the proper extraction of individual near end crosstalk (NEXT), far end crosstalk (FEXT), and other interesting transfer functions (like phantom and split-pair transfer functions) from the MIMO matrix model, and provides simple explanations of some observed effects in measured NEXT and FEXT.

The limitations of previous research justify this additional work. Past transmission practice within binder cables was based on differential excitation of individual pairs. Thus, channel studies focused on characterizing wire pairs under differential excitations. These studies did not treat cable binders as MIMO channels. Nevertheless, previous research generated many interesting results and methods that prepare us for the binder MIMO model of this paper: particularly, methods on modeling twisting for twisted pair cables [7], [8], on the importance of cable imperfections [9], [10], and empirical power-sum crosstalk characterization [11]. This paper's proposed binder MIMO model extends previous twisting models from single twisting rate per pair to a cable binder comprising lines with different twisting rates, and incorporates cable imperfections. It presents systematic methods to obtain the MIMO channel matrix from basic cable parameters and source–load impedance configurations.

This paper is organized as follows. Section II introduces the modeling of $2N$ wires or N pairs. Matrix RLCG models are used to characterize an incremental section following Paul's [4] general treatment of this subject. Terminology is introduced that directly parallels the well-known scalar RLCG models. Section II also investigates the appropriate matrix sources and loads, and their construction, definition, and relation to traditional N

Paper approved by C.-L. Wang, the Editor for Transmission Systems of the IEEE Communications Society. Manuscript received June 28, 2004; revised September 30, 2006 and February 6, 2007. This work was supported in part by the France Télécom R&D.

B. Lee was with the Department of Electrical Engineering, Stanford University, Stanford, CA 94305 USA. He is now an individual consultant (e-mail: lee_bin@hotmail.com).

J. M. Cioffi, and S. Jagannathan are with the Department of Electrical Engineering, Stanford University, Stanford, CA 94305 USA (e-mail: binlee@stanford.edu; cioffi@stanford.edu; sumanthj@stanford.edu).

K. Seong is with Qualcomm, Inc., San Diego, CA 92121 USA. He is also with Stanford University, Stanford, CA 94305 USA (e-mail: kibeoms@qualcomm.com).

Y. Kim is with Texas Instruments, Inc., Dallas, TX 75243 USA (e-mail: youngjae@stanfordalumni.org).

M. Mohseni and M. H. Brady are with ASSIA, Inc., Redwood City, CA 94065-1198 USA (e-mail: mmohseni@assia-inc.com; mbrady@assia-inc.com).

Digital Object Identifier 10.1109/TCOMM.2007.902597

independent differential excitations. An interesting result is that traditional, scalar, and differential source and load matching corresponds to an unusual singular situation that is not well matched in the case of MIMO. Section II then also lays a foundation for cascades of binder sections that not only allow the modeling of traditional gauge changes and "bridged taps" but also allow the modeling of twisting and binder imperfections like twist-rate variation and pair-center-separation variation. Section III shows that perfect twisting, indeed, almost entirely eliminates any crosstalk and that imperfect twisting causes actual measured crosstalk to be several orders larger than what would be produced by perfect twisting. Section III also includes a few basic comparisons of actual measured channel transfer characteristics and computed characteristics, providing a strong indication of the model's potential use in the modeling of MIMO binder transmission. Section IV concludes the paper.

II. Binder MIMO Channel

The goal of the binder MIMO channel model is to obtain channel characteristics for closely packed pairs in a binder. Using MIMO theory, the channel response can be expressed as

$$\mathbf{Y} = \mathbf{H}\mathbf{X} + \mathbf{N} \tag{1}$$

where $\mathbf{X}$ is an input column vector, $\mathbf{Y}$ is an output column vector, and $\mathbf{N}$ denotes the noise components including impulse noise, radio frequency noise, and other background noise. The binder MIMO channel model provides a method to calculate $\mathbf{H}$ from physical system parameters. The direct-line transfer function, NEXT, and FEXT for the commonly used differential excitation and reception can be easily calculated using $\mathbf{H}$.

The binder MIMO channel model uses two concepts: circuit theory and cable geometric modeling. The circuit theory is used to derive voltage–current input–output relations for a cable system. Such derivations require per-unit-length circuit elements that will be provided by cable geometry modeling. This section first presents the circuit theory for a binder MIMO channel, followed by a treatment of the cable geometry modeling.

A. Circuit Theory for a Binder MIMO Channel

The circuit theory for a binder MIMO channel is based on multiconductor transmission line (MTL) theory [4]. This approach elucidates that proper source or load matrices may be more appropriate at both ends of the cable, if possible to implement. To apply the theory, a cable loop is treated as a cascade of many segments. Within each segment, the positions of the conductors are fixed, and the positions can vary between segments in order to incorporate twisting and cable imperfections in the model. This section first applies MTL theory to a cable segment to obtain voltage–current input–output relations for such a segment; then, the binder MIMO transfer matrix for the system can be calculated for the given source–load configuration. A designer may then cascade sections, multiplying matrix transfer functions to generate the individual NEXT, FEXT, and direct-line transfer functions for the entire binder. This section also includes a discussion of split-pair and phantom transfer functions. All these theories assume that certain matrix resistance ($\mathbf{R}$), inductance ($\mathbf{L}$), capacitance ($\mathbf{C}$), and conductance ($\mathbf{G}$) values are known for each segment. Models for these matrices appear at the end of this section. Methods to obtain $\mathbf{R}$, $\mathbf{L}$, $\mathbf{C}$, and $\mathbf{G}$ for given geometry configuration are also included.

1) MTL Theory for a Cable Segment: In MTL theory, the small segment of cable shown in Fig. 1(a) can be characterized by matrix parameters $\mathbf{R}$, $\mathbf{L}$, $\mathbf{C}$, and $\mathbf{G}$. Four conductor wires are used in the following discussions for simplicity of illustration. All results and formulas are easily extendable to more wires. In a four-wire cable, one wire can be selected as a common reference; then, the input–output characteristics for the cable can be completely modeled using three voltages and three currents. To describe this transmission line, four incremental resistances, six capacitances, six inductances, and six conductances are required. Fig. 1(a) shows the labeling and indexing of these circuit elements.

The input–output voltage and current relations for a cable segment can be characterized by a transfer matrix $\mathbf{\Phi}$, as in the following formulas:

$$\begin{bmatrix} \mathbf{V}(z,\omega) \\ \mathbf{I}(z,\omega) \end{bmatrix} = \mathbf{\Phi}(z,d,\omega) \begin{bmatrix} \mathbf{V}(z+d,\omega) \\ \mathbf{I}(z+d,\omega) \end{bmatrix} \tag{2}$$

$$\mathbf{\Phi}(z,d,\omega) = \begin{bmatrix} \mathbf{A}(z,d,\omega) & \mathbf{B}(z,d,\omega) \\ \mathbf{C}(z,d,\omega) & \mathbf{D}(z,d,\omega) \end{bmatrix} \tag{3}$$

where $\mathbf{V}(z)$ and $\mathbf{I}(z)$ are the column vectors, z is the starting position of the cable segment, and d is the length of the segment under consideration. $\mathbf{A}$, $\mathbf{B}$, $\mathbf{C}$, and $\mathbf{D}$ are 3×3 matrices that are functions of the resistance, inductance, conductance, capacitance, the cable geometry, and its physical properties. The position and frequency dependence of $\mathbf{A}$, $\mathbf{B}$, $\mathbf{C}$, $\mathbf{D}$, $\mathbf{V}$, $\mathbf{I}$, and $\mathbf{\Phi}$ are explicitly shown in these formulas. The position dependence becomes important when twisting [see Fig. 1(b)] and cable imperfections are included in the model. Due to the position dependence, these matrices will vary from segment to segment. In the rest of the paper, notation for explicit frequency dependence is dropped for convenience. Furthermore, without loss of generality, it is assumed that $z = 0$.

In general, a cable segment can be described by a position-dependent transmission-line equation. In practical cable systems, $\mathbf{L}$, $\mathbf{C}$, and $\mathbf{G}$ are slowly varying with distance along the cable; thus, a position-independent transmission line equation can be used for each segment. For channel-modeling purposes, the position-invariant transmission-line equations for each segment are [4], [5]

$$\begin{aligned} -\frac{d\mathbf{V}}{dz} &= (\mathbf{R} + j\omega\mathbf{L}) \cdot \mathbf{I} = \mathbf{Z} \cdot \mathbf{I} \\ -\frac{d\mathbf{I}}{dz} &= (\mathbf{G} + j\omega\mathbf{C}) \cdot \mathbf{V} = \mathbf{Y} \cdot \mathbf{V} \end{aligned} \tag{4}$$

where $\mathbf{Z} = \mathbf{R} + j\omega\mathbf{L}$ is the symmetric per-unit-length impedance matrix and $\mathbf{Y} = \mathbf{G} + j\omega\mathbf{C}$ is the symmetric per-unit-length admittance matrix. The explicit matrix forms of $\mathbf{R}$, $\mathbf{L}$, $\mathbf{C}$, and $\mathbf{G}$ are given in Fig. 1(a). The input–output relation for voltage and current, as well as $\mathbf{\Phi}$, can be solved for each segment

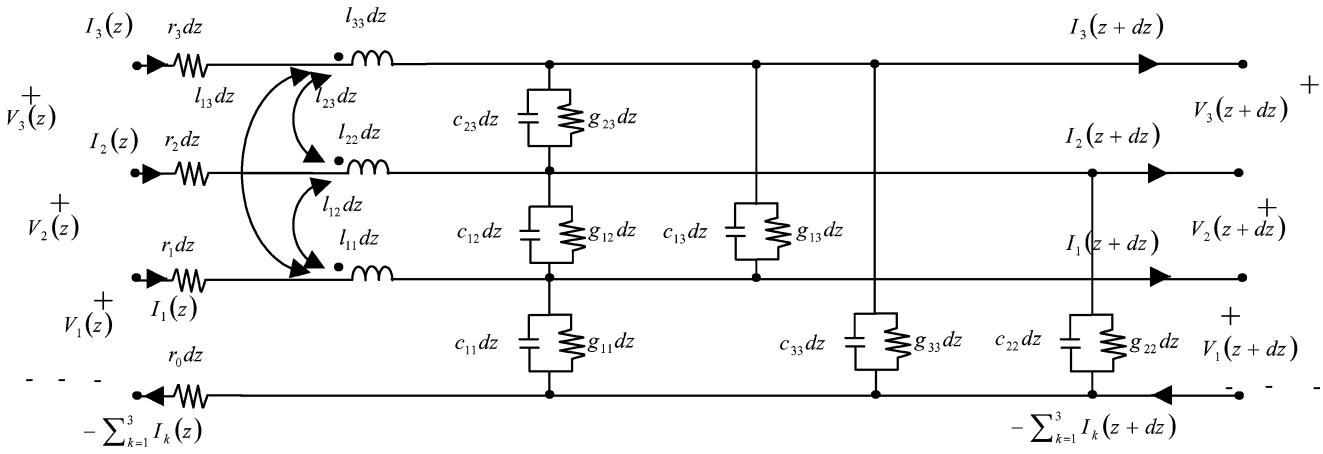

$$\mathbf{R}=\begin{bmatrix} r_0+r_3 & r_0 & r_0 \\ r_0 & r_0+r_2 & r_0 \\ r_0 & r_0 & r_0+r_1 \end{bmatrix} \quad \mathbf{L}=\begin{bmatrix} l_{33} & l_{23} & l_{13} \\ l_{23} & l_{22} & l_{12} \\ l_{13} & l_{12} & l_{11} \end{bmatrix} \quad \mathbf{C}=\begin{bmatrix} c_{13}+c_{23}+c_{33} & -c_{23} & -c_{13} \\ -c_{23} & c_{12}+c_{23}+c_{22} & -c_{12} \\ -c_{13} & -c_{12} & c_{13}+c_{12}+c_{11} \end{bmatrix}$$

$$\mathbf{G}=\begin{bmatrix} g_{13}+g_{23}+g_{33} & -g_{23} & -g_{13} \\ -g_{23} & g_{12}+g_{23}+g_{22} & -g_{12} \\ -g_{13} & -g_{12} & g_{13}+g_{12}+g_{11} \end{bmatrix}$$

(a)

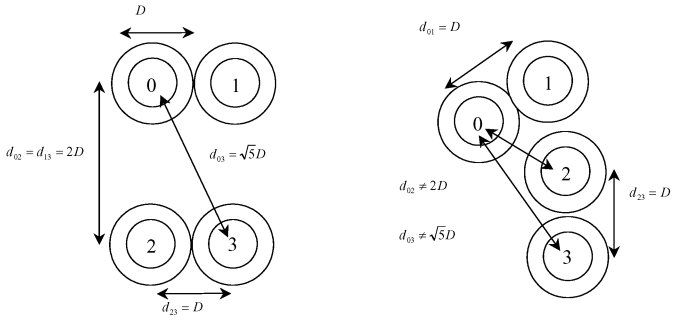

(b)

Fig. 1. (a) Segment of cable binder can be described with **R**, **L**, **C**, **G**, **V**, and **I**. (b) Distance between pairs (and thus the LCG values) varies with twisting.

by extending the well-known two-port theory results [12], [13]:

$$\begin{bmatrix} \mathbf{V}(0) \\ \mathbf{I}(0) \end{bmatrix} = \begin{bmatrix} \cosh(\boldsymbol{\gamma} d) & \sinh(\boldsymbol{\gamma} d)\cdot\mathbf{Z}_0 \\ \sinh(\boldsymbol{\gamma}^T d)\cdot\mathbf{Z}_0^{-1} & \cosh(\boldsymbol{\gamma}^T d) \end{bmatrix} \cdot \begin{bmatrix} \mathbf{V}(d) \\ \mathbf{I}(d) \end{bmatrix} = \boldsymbol{\Phi}(d) \begin{bmatrix} \mathbf{V}(d) \\ \mathbf{I}(d) \end{bmatrix} \tag{5}$$

$$\boldsymbol{\Phi}(d) = \begin{bmatrix} \cosh(\boldsymbol{\gamma} d) & \sinh(\boldsymbol{\gamma} d)\cdot\mathbf{Z}_0 \\ \sinh(\boldsymbol{\gamma}^T d)\cdot\mathbf{Z}_0^{-1} & \cosh(\boldsymbol{\gamma}^T d) \end{bmatrix} \tag{6}$$

$$\mathbf{Z}_0 = \mathbf{Z}\cdot\boldsymbol{\gamma}^{-T} = \mathbf{Y}^{-1}\cdot\boldsymbol{\gamma}^T = \boldsymbol{\gamma}^{-1}\cdot\mathbf{Z} = \boldsymbol{\gamma}\cdot\mathbf{Y}^{-1} \tag{7}$$

$$\mathbf{ZY} = \boldsymbol{\gamma}^2 = (-\boldsymbol{\gamma})^2 = (\mathbf{R}+j\omega\mathbf{L})\cdot(\mathbf{G}+j\omega\mathbf{C}) \tag{8}$$

where $\mathbf{Z}_0$ is the characteristic impedance matrix and $\boldsymbol{\gamma}$ is the propagation constant matrix for the segment. The matrices $\mathbf{Z}_0$ and $\boldsymbol{\gamma}$ are position dependent and vary between segments. The matrices **A**, **B**, **C**, and **D** for one segment, defined in (3), can be obtained by a one-to-one mapping with (5).

A complete cable can be treated as a cascade of segments both for mathematical convenience and to model a practical cable structure. By modeling a complete cable loop as a cascade of segments, the input–output transfer function for the cable is then

$$\begin{bmatrix} \mathbf{V}(0) \\ \mathbf{I}(0) \end{bmatrix} = \boldsymbol{\Phi}_1\cdot\boldsymbol{\Phi}_2\cdots\boldsymbol{\Phi}_N\cdot\begin{bmatrix} \mathbf{V}(l) \\ \mathbf{I}(l) \end{bmatrix} = \boldsymbol{\Phi}\cdot\begin{bmatrix} \mathbf{V}(l) \\ \mathbf{I}(l) \end{bmatrix} \tag{9}$$

where $\boldsymbol{\Phi}_i$ describes the input–output transfer function for one segment, l is the length of a full cable, and N is the total number of segments under consideration. If each section of the cable has the same length d, then $l = Nd$. Again, an overall $\boldsymbol{\Phi}$ can be written in terms of the matrices **A**, **B**, **C**, and **D**, which are

equal-size square matrices

$$\mathbf{\Phi} = \begin{bmatrix} \mathbf{A} & \mathbf{B} \\ \mathbf{C} & \mathbf{D} \end{bmatrix}. \tag{10}$$

Once $\mathbf{A}$, $\mathbf{B}$, $\mathbf{C}$, $\mathbf{D}$, and $\mathbf{\Phi}$ are obtained, it is easy to obtain the MIMO channel transfer function as shown in the sequel.

2) MIMO Channel Transfer Function: To calculate the MIMO channel transfer function, an input–output voltage transfer function needs to be calculated. The input–output voltage matrix transfer function $\mathbf{T}$ for a cable is defined by

$$\mathbf{V}(l) = \mathbf{T} \cdot \mathbf{V}(0) \tag{11}$$

where $\mathbf{V}(0)$ is the input voltage vector to the cable and $\mathbf{V}(l)$ is the output voltage vector of the cable. The output voltage vector is related to output current vector by the load admittance matrix $\mathbf{Y}_L$ by

$$\mathbf{I}(l) = \mathbf{Y}_L \cdot \mathbf{V}(l). \tag{12}$$

Using (9)–(12), $\mathbf{T}$ can be computed as

$$\mathbf{T} = (\mathbf{A} + \mathbf{B}\mathbf{Y}_L)^{-1}. \tag{13}$$

This formula uses the admittance matrix instead of the impedance matrix because the impedance matrix does not exist under the traditional differential load. To get the voltage transfer function between a source and a load, a voltage divider between the source admittance and the input admittance to the cable needs to be considered. The input admittance $\mathbf{Y}_1$ is defined by $\mathbf{I}(0) = \mathbf{Y}_1 \cdot \mathbf{V}(0)$, where $\mathbf{I}(0)$ and $\mathbf{V}(0)$ are the input current and voltage vectors to cable. The formula for the input admittance is given by

$$\mathbf{Y}_1 = (\mathbf{C} + \mathbf{D} \cdot \mathbf{Y}_L) \cdot (\mathbf{A} + \mathbf{B} \cdot \mathbf{Y}_L)^{-1}. \tag{14}$$

The transfer function $\mathbf{H}(f)$ between an input voltage supply vector $\mathbf{V}_S$ (with a finite internal series impedance matrix $\mathbf{Z}_S$) and the output voltage $\mathbf{V}_L$ [$= \mathbf{V}(d)$] can be calculated by considering $\mathbf{Y}_S$, $\mathbf{Y}_1$, and $\mathbf{T}$:

$$\mathbf{H} = \mathbf{T} \cdot (\mathbf{Y}_1 + \mathbf{Y}_S)^{-1} \cdot \mathbf{Y}_S. \tag{15}$$

This formula generates the MIMO channel transfer function $\mathbf{H}$ as in $\mathbf{Y} = \mathbf{H}\mathbf{X} + \mathbf{N}$ if the input and output are voltage vectors. When one wire is chosen as a common reference in a system with $2N$ conductor wires, this method produces a $(2N-1) \times (2N-1)$ MIMO channel. The channel derived in this way is referred to as a *common-mode MIMO channel*. The MIMO channel model works for any source and load admittance ($\mathbf{Y}_S$ and $\mathbf{Y}_L$) (or impedance $\mathbf{Z}_S$ and $\mathbf{Z}_L$) provided the matrix inverses in (13), (14), and (15) exist. An interesting choice of load and source impedance matrices is as follows.

i) $\mathbf{Z}_L = \mathbf{Z}_0(l)$, load matches the matrix characteristic impedance.
ii) $\mathbf{Z}_s = \mathbf{Z}_0(0)$, source matches the matrix characteristic impedance.

Here $\mathbf{Z}_0(l)$ is the matrix characteristic impedance of cable at the load end and $\mathbf{Z}_0(0)$ is the matrix characteristics impedance at the source end.

These matching matrices are particularly meaningful when $\mathbf{Z}_0$ is independent of cable position as for perfect "quad" cables when neighboring quads are neglected.[1] In such cables, load matrix matching completely removes the well-known ripples in NEXT vs. frequency curves. In general, $\mathbf{Z}_L$ and $\mathbf{Z}_s$ in these formulas depend on frequency. However, for real cable systems, $\mathbf{Z}_0$ is almost purely resistive above a few hundred kilohertz. Therefore, it is easy to obtain matrix impedance matching at frequencies above a few hundred kilohertz. For twisted pair cable, because $\mathbf{Z}_0$ is position dependent, $\mathbf{Z}_L = \mathbf{Z}_0(l)$ or $\mathbf{Z}_s = \mathbf{Z}_0(0)$ only ensures the load or source impedance matching either at the load end or at the source end, but not for the whole cable. In general, load matrix matching cannot completely remove ripples in NEXT vs. frequency curves as it does for the "quad" cable. For both the "quad" cable and the twisted pair cable, a simpler load–source configuration is to choose $\mathbf{Z}_L$ and $\mathbf{Z}_s$ to be diagonal matrices.

The common-mode MIMO channel is intuitively the default MIMO channel for a binder cable; but a practical communication system that uses such a channel may be complicated to implement, and may require sophisticated noise cancellation methods under noisy conditions. A simpler MIMO model for the binder cable exists based on differential excitations and receptions, where sources and loads are individually applied to each pair of conductor wires. The differential excitations and receptions combined with twisting of pairs also significantly reduce crosstalk and noise coupling. In this configuration, FEXT can be defined between pairs and a direct transfer function can be defined for each pair. For a cable system with N pairs (or $2N$ wires), a channel matrix can be defined for such a source–load configuration. In the channel matrix, the direct transfer functions for pairs are in the diagonal positions and FEXT is in the off-diagonal positions. The channel derived in this way is referred to as a *simplified differential mode MIMO channel*. For example, with four conductor wires forming two differential pairs, the differential mode MIMO channel matrix $\mathbf{H}_{sd}$ is

$$\mathbf{H}_{sd} = \begin{bmatrix} T_1 & \text{FEXT}_{12} \\ \text{FEXT}_{21} & T_2 \end{bmatrix} \tag{16}$$

where T_1 and T_2 are direct transfer functions of each pair, and FEXT_{12} and FEXT_{21} are the FEXT transfer functions induced by one pair to the other pair. In practice, implementing an $N \times N$ differential mode MIMO system is less complicated than is implementing a $(2N-1) \times (2N-1)$ common-mode MIMO system. The tradeoff is that the system formed by $2N$ conductor wires has higher channel capacity if the system is modeled as a $(2N-1) \times (2N-1)$ channel rather than an $N \times N$ channel [1], [2].

Since the source–load voltage relation is given by the matrix transfer function $\mathbf{H}$, FEXT as well as NEXT and the direct-line transfer functions can be calculated from $\mathbf{H}$ under differential loads and sources.

3) Computation of Scalar Direct-Line and Crosstalk Transfer Functions With Differential Source and Load Impedances: Fig. 2 illustrates a typical situation where excitations are scalar voltages, and load and source impedances are differential for

[1] "Quad" cables are used in France, Germany, and other countries.

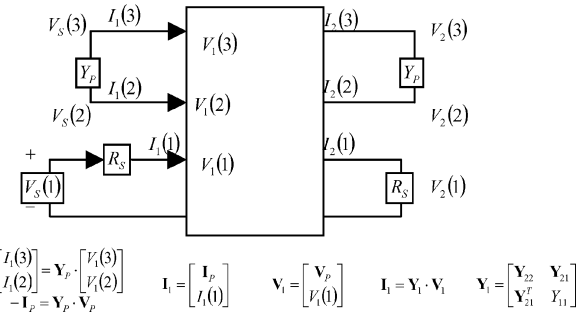

Fig. 2. Scalar sources and differential loads.

two lines. Y_p is the admittance of the loads placed across each and every pair, and other quantities are defined by the equations at the bottom of Fig. 2. $\mathbf{Y}_P$ is a 2×2 admittance matrix specified in the figure for the two-port network between wires 2 and 3. The known admittance matrix $\mathbf{Y}_1$ (defined in Fig. 2) can be used to calculate all scalar transfer functions. The basic circuit equation is

$$-\mathbf{Y}_P \cdot \mathbf{V}_P = \mathbf{Y}_{22} \cdot \mathbf{V}_P + \mathbf{Y}_{21} \cdot V_1(1) \tag{17}$$

from which one obtains

$$\mathbf{V}_P = -(\mathbf{Y}_P + \mathbf{Y}_{22})^{-1} \cdot \mathbf{Y}_{21} \cdot V_1(1). \tag{18}$$

For a differential source where all pairs use the same source impedance,

$$Y_P = \begin{bmatrix} \frac{1}{R_S} & -\frac{1}{R_S} \\ -\frac{1}{R_S} & \frac{1}{R_S} \end{bmatrix}$$

which is singular. The relation between the scalar source voltage and the network's input voltage is

$$V_S(1) = R_S \cdot I_1(1) + V_1(1) = [1 + R_S \cdot y_1] \cdot V_1(1) \tag{19}$$

$$V_1(1) = \frac{V_S(1)}{1 + R_S \cdot y_1}. \tag{20}$$

Then, the NEXT transfer function is calculated from (18) and (20) as

$$H_{\text{NEXT}} = \frac{V_1(3) - V_1(2)}{V_S(1)} = [-1 \quad 1] \cdot \frac{(\mathbf{Y}_P + \mathbf{Y}_{22})^{-1} \cdot \mathbf{Y}_{21}}{1 + R_S \cdot y_1} \tag{21}$$

while the matrix transfer function $\mathbf{T}$ from (13) is additionally used to calculate the FEXT transfer function

$$H_{\text{FEXT}} = \frac{V_2(3) - V_2(2)}{V_S(1)} = [1 \quad -1 \quad 0] \cdot \frac{\mathbf{T}}{1 + R_S \cdot y_1} \cdot \begin{bmatrix} -(\mathbf{Y}_P + \mathbf{Y}_{22})^{-1} \cdot \mathbf{Y}_{21} \\ 1 \end{bmatrix} \tag{22}$$

and the main source to load transfer function is

$$H = \frac{V_2(1)}{V_S(1)} = [0 \quad 0 \quad 1] \cdot \frac{\mathbf{T}}{1 + R_S \cdot y_1} \cdot \begin{bmatrix} -(\mathbf{Y}_P + \mathbf{Y}_{22})^{-1} \cdot \mathbf{Y}_{21} \\ 1 \end{bmatrix}. \tag{23}$$

The other three NEXT and three FEXT transfer functions can be computed by reindexing the wires and repeating the procedure. Equations (17)–(20) are valid for any number of lines in which case the quantities $\mathbf{V}_P$, $\mathbf{I}_P$, $\mathbf{Y}_P$, $\mathbf{Y}_{22}$, and $\mathbf{Y}_{21}$ become $(2N-2)$-dimensional. The leading vectors on the right-hand sides of (21) and (22) have two nonzero entries $+1$ and -1 in the positions of the line into which the crosstalk is being computed. The leading vector in (23) has all zeros except a 1 in the last (right most) position.

These methods to extract information for differential loads from a common-mode MIMO channel matrix can be applied not only to traditional differential excitation, but also to unconventional differential excitations. There are interesting relations among these excitations.

4) Relation To Traditional Models Involving Differential Excitations and Phantom Components: Fig. 3 shows three views of the same two-twisted pair cable.

1) Description with all voltages referenced to an external reference (e.g., earth ground) (top)
2) Traditional "symmetric" description using differential excitations and phantom components (left)
3) Asymmetric description of this section that allows direct matrix RLCG models (right)—some of the direct transfer functions are between the wires of different twisted pair, which are sometimes called "split-pair" transfer functions.

The relationship between the models is listed in the figure. The three voltages of the traditional symmetric model can be related (input or output) to the three voltages of the asymmetric model. The symmetric model includes a third voltage ΔV_p that is often colloquially called a "phantom" signal (this name is unfortunate because this voltage exists and can be very real in its effects). The phantom component ΔV_p is defined as $\Delta V_p = \Delta V_2 - \Delta V_1$. The concept of the phantom component is very useful if one would like to use the third transmission mode, which is available in the asymmetric voltage model, in systems that are already using differential mode transmission. An extra circuit can be implemented on top of the existing differential excitation and reception to utilize this extra mode. For N pairs, $N-1$ phantom modes could be used along with the existing differential mode transmission in order to implement the overall $(2N-1) \times (2N-1)$ MIMO channel, which would otherwise require completely changing the terminations of existing systems. Any transfer functions involving differential and/or phantom components in traditional modeling can always be directly related to transfer functions based on asymmetric voltages and vice versa (Table I). The two are completely equivalent, and no extra information appears in one with respect to the other (however, some could be easier to measure or use than others in practice). A fourth voltage occurs in the absolute voltage model (top of Fig. 3), and would represent a possible transmission mode with respect to earth ground. However, this mode is not modeled in either symmetric or asymmetric approaches, and is not used in present DSL transmission systems.

The aforementioned discussions show that for a cable system with given source–load configuration, if the channel matrix $\mathbf{H}$ is known, the magnitude and the phase of individual NEXT, FEXT, split-pair, and phantom transfer functions can all be calculated.

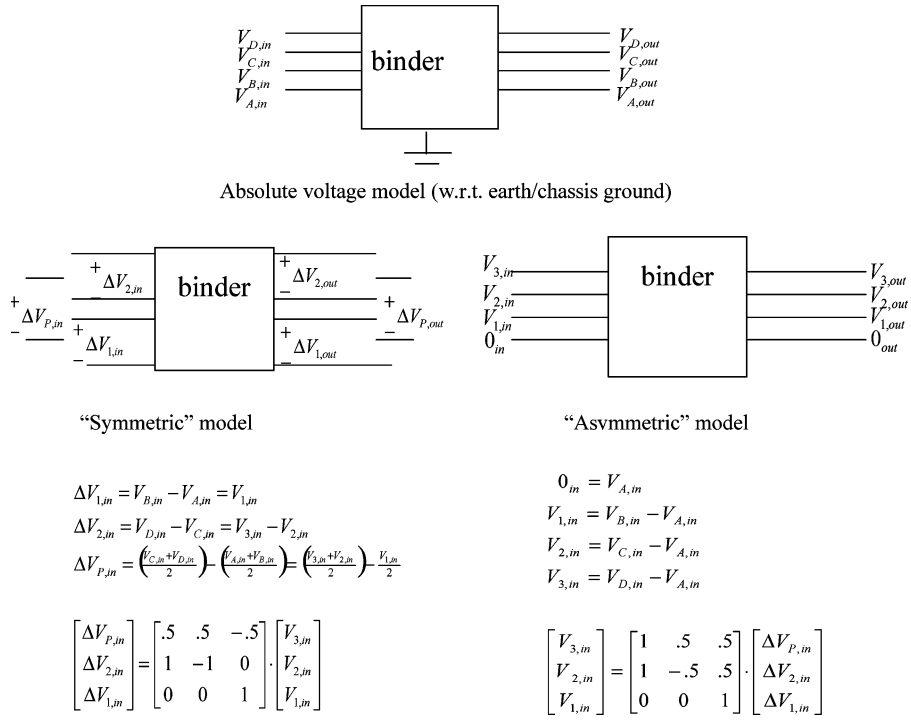

$$\Delta V_{1,in} = V_{B,in} - V_{A,in} = V_{1,in}$$
$$\Delta V_{2,in} = V_{D,in} - V_{C,in} = V_{3,in} - V_{2,in}$$
$$\Delta V_{P,in} = \left(\frac{V_{C,in}+V_{D,in}}{2}\right) - \left(\frac{V_{A,in}+V_{B,in}}{2}\right) = \left(\frac{V_{3,in}+V_{2,in}}{2}\right) - \frac{V_{1,in}}{2}$$

$$\begin{bmatrix}\Delta V_{P,in}\\ \Delta V_{2,in}\\ \Delta V_{1,in}\end{bmatrix} = \begin{bmatrix}.5 & .5 & -.5\\ 1 & -1 & 0\\ 0 & 0 & 1\end{bmatrix}\cdot\begin{bmatrix}V_{3,in}\\ V_{2,in}\\ V_{1,in}\end{bmatrix}$$

$$0_{in} = V_{A,in}$$
$$V_{1,in} = V_{B,in} - V_{A,in}$$
$$V_{2,in} = V_{C,in} - V_{A,in}$$
$$V_{3,in} = V_{D,in} - V_{A,in}$$

$$\begin{bmatrix}V_{3,in}\\ V_{2,in}\\ V_{1,in}\end{bmatrix} = \begin{bmatrix}1 & .5 & .5\\ 1 & -.5 & .5\\ 0 & 0 & 1\end{bmatrix}\cdot\begin{bmatrix}\Delta V_{P,in}\\ \Delta V_{2,in}\\ \Delta V_{1,in}\end{bmatrix}$$

Fig. 3. Equivalence of traditional symmetric model and asymmetric model.

Additionally, for a given source–load configuration, if **R**, **L**, **C**, and **G** matrices are known for each segment, then the channel matrix **H** can be obtained. Thus, to complete the model, methods to find **R**, **L**, **C**, and **G** matrices for each cable segment are needed.

*5) Calculations of **R**, **L**, **C**, and **G** Matrices:* For a given cable geometry, two methods can be used to obtain the per-unit-length **R**, **L**, **C**, and **G** matrices. One method is based on an analytical approach using basic electromagnetic theory; another method is based on extracting matrix elements from measured data. Calculation of **R**, **L**, **C**, and **G** directly from the basic electromagnetic principle inevitably involves some approximations. Established methods with various levels of approximation can be found in [4], [13], and [14]. One disadvantage of the calculation approach is that it requires knowing the physical constants $\mu, \varepsilon_r,$ **and** σ (permittivity, permeability, and conductivity, respectively) of the dielectric filling material of cables and the conductivity of metal conductors. These values may not be easy to obtain or estimate. In addition, the permittivity of the insulation material may also vary across the cable cross section [23]. The approach based on extracting **R**, **L**, **C**, and **G** from measurements overcomes such difficulties [12]. However, there are drawbacks to this approach. Typically, the frequency-dependent characteristics of a single pair are measured for an isolated twisted pair. In other words, twisted pairs were not in a cable binder, so the measured values are not completely suitable for actual twisted pairs inside a cable binder; therefore, this approach only works as an alternative approximation. In actual simulations, both methods can be implemented, and when some measured data are available, one method may be favored over another. Both approaches depend on knowing cable geometric parameters. Therefore, the proposed binder MIMO model includes the following cable geometric models.

B. Cable Geometric Model

To calculate **R**, **L**, **C**, and **G** matrices, the actual cable geometry needs to be considered. Two types of geometric configurations are discussed in this section: "quad" cables and twisted pair cables. It can be shown theoretically [10], [15], [19]–[26], and confirmed by simulations in this work, that cable imperfections are important to characterize the channel. So, for each type of cable, geometric modeling also contains cable imperfection modeling.

1) Geometric Modeling of Quad Cables: An ideal "single quad" has nice symmetry properties. The four wires in a perfect quad are parallel to each other, and the centers of the four wires form a square. This symmetry ensures that crosstalk under normal differential excitation is zero when the source and load impedances are set up over one diagonal pair and crosstalk is measured over the other diagonal pair. In real imperfect quads, the centers of the four wires do not form a perfect square. Thus, the expected symmetry is imperfect. The quads also rotate along the cable. The rotation does not affect the crosstalk characteristics among four conductor wires in the same quad, but does reduce the crosstalk between different quads much like twisting reduces crosstalk between twisted pairs. A description of the geometry of a single quad requires only the positions of the four conductor centers and the conductor radii. Modeling multiple quads within a binder follows the same procedure as described next for twisted pair cables.

2) Geometric Modeling of the Twisted Pair Cable: An accurate geometric model of a twisted pair cable is difficult to

TABLE I
RESULTS FOR SYMMETRIC AND ASYMMETRIC MODE

15 Transfer functions of interest for 3x3 Case – G is used for NEXT and H for FEXT (first subscript is output and second subscript is input)		
Label	**Symmetric**	**Asymmetric**
Direct transfer functions	$\frac{\Delta V_{1,out}}{\Delta V_{1,in}}$	$\frac{V_{1,out}}{V_{1,in}} = H_{11}$
	$\frac{\Delta V_{2,out}}{\Delta V_{2,in}}$	$\frac{V_{3,out} - V_{2,out}}{V_{3,in} - V_{2,in}} = \frac{H_{32} - H_{22}}{G_{32} - 1}$
FEXT transfer functions	$\frac{\Delta V_{2,out}}{\Delta V_{1,in}}$	$H_{31} - H_{21}$
	$\frac{\Delta V_{1,out}}{\Delta V_{2,in}}$	$\frac{H_{12}}{G_{32} - 1}$
NEXT transfer functions	$\frac{\Delta V_{2,in}}{\Delta V_{1,in}}$	G_{21}
	$\frac{\Delta V_{1,in}}{\Delta V_{2,in}}$	G_{12}
Phantom FEXT transfer functions	$\frac{\Delta V_{2,out}}{\Delta V_{P,in}}$	$\frac{2(H_{31} - H_{21})}{G_{31} + G_{32} - 1}$
	$\frac{\Delta V_{1,out}}{\Delta V_{P,in}}$	$\frac{2(H_{11})}{G_{31} + G_{32} - 1}$
	$\frac{\Delta V_{P,out}}{\Delta V_{2,in}}$	$\frac{H_{32} + H_{22} - H_{12}}{2(G_{32} - 1)}$
	$\frac{\Delta V_{P,out}}{\Delta V_{1,in}}$	$\frac{H_{31} + H_{21} - H_{11}}{2}$
Phantom Direct transfer functions	$\frac{\Delta V_{P,out}}{\Delta V_{p,in}}$	$\frac{H_{31} + H_{21} - H_{11}}{G_{31} + G_{21} - 1}$
Phantom NEXT transfer functions	$\frac{\Delta V_{2,in}}{\Delta V_{P,in}}$	$\frac{2(G_{31} - G_{21})}{G_{31} + G_{32} - 1}$
	$\frac{\Delta V_{1,in}}{\Delta V_{P,in}}$	$\frac{2}{G_{31} + G_{32} - 1}$
	$\frac{\Delta V_{P,in}}{\Delta V_{2,in}}$	$\frac{G_{32} + G_{22} - G_{12}}{2(G_{32} - 1)}$
	$\frac{\Delta V_{P,in}}{\Delta V_{1,in}}$	$G_{31} + G_{21} - 1$

obtain; therefore, simplifications are inevitable for the purpose of practical modeling and simulation. This section presents approximations that are used to compare with measurements in this paper. These approximations are chosen not only because they are relatively simple to implement, but also because simulations based on these approximations reveal typical crosstalk characteristics observed in measurements.

Modeling the geometry of a twisted pair includes a description of the twisting and the associated imperfections. To describe the twisting of a pair, the trajectory of the pair center as well as the relative rotations of two wires w.r.t. the pair center are required. Different levels of approximation have been proposed in the past to describe twisting [7], [8], [16]. For simulation purposes, in this paper, the single-pair discrete-rotation model [16] is extended to multiple-pair discrete rotation [15], where every pair in a twisted cable is modeled as discretely rotating. The modeling of binder MIMO imperfections in this paper mainly considers three types of cable imperfections: pair center variations, twist-rate variations, and nontwisted segment at the cable head or tail. These effects together can be used to model the variation of relative distance between pairs.

a) Type I Imperfection in Twisted Pair Cables: Pair Center Variation: The pair-center variation denotes the situation in which the pair centers deviate from the expected position. For an ideal parallel layout of twisted pairs, the centers of any two pairs form parallel straight lines, and the distance between the two wire centers in each twisted pair is fixed. This ideal cable is called a "perfect twisted pair cable" in this paper. It can be analytically proved that electromagnetic coupling between perfect twisted pairs is almost entirely canceled under normal differential excitation [15]. In reality, because manufacturing procedures are not perfect and twisted pairs are densely packed inside cables, pair centers cannot form straight parallel lines, and thus, pair center separation varies. In order to model this effect, the centers of the twisted pairs are varied along the cable length, thereby inherently capturing the position-dependent separation between the different twisted pairs. The centers of the twisted pairs can be modeled as two-dimensional vectors at each distance z along the cable. The following model applies independently to both components of the pair center vector.

Let $\mathrm{pc}(i,z)$ denote any component of the center of pair i along the cable of length z:

$$\mathrm{pc}(i,z) = \overline{\mathrm{pc}}(i,z) + \Delta\mathrm{pc}(i,z) \tag{24}$$

where i is an index for each pair in a twisted pair cable, $\overline{\mathrm{pc}}(i,z)$ is the expected pair center position for pair i at the cable of length z, and $\Delta\mathrm{pc}(i,z)$ is the deviation from the expected position. For nonparallel wires within the cable, $\overline{\mathrm{pc}}(i,z)$ can be described by known parameters. In this paper, two pair-center variation methods are examined, and are used to compare with measurements: a random variation method and a sinusoidal variation method. In the case of random variation,

$$\Delta\mathrm{pc}(i,z) = \alpha(i,z) \cdot \overline{\mathrm{pc}}_0(i) \tag{25}$$

where $\alpha(i,z)$ is a random function of z. For a practical twisted pair cable structure, it was observed via simulations that the value of $\alpha(i,z)$ is most likely in the range of [0, 0.15]; $\overline{\mathrm{pc}}_0(i)$ is the average of the pair center position. For the sinusoidal variation,

$$\Delta\mathrm{pc}(i,z) = \alpha_i \sin(k_i \cdot z) \cdot \overline{\mathrm{pc}_0}(i) \tag{26}$$

where α_i is a constant for a pair and k_i denotes the space frequency. In the case of the single pair discrete rotation model, k_i is the reciprocal of the twist rate tr of the pair. In this paper, the twist rate of a twisted pair is defined as the average space period of the twisted pair (in the length of meter or inch). For the two-pair or the multipair discrete-rotation model, k_i can be obtained from the geometric cable structure. Simulations show that $0 < \alpha_i < 0.2$ works for many practical twisted pair cable structures. A few more sophisticated pair-center variation options have been investigated to include the "squeezing" effect from the neighboring pairs; however, their improvements were negligible, and so, are not further considered. The net effect of pair-center variation is that such variation breaks the electromagnetic-coupling cancellation mechanism inside a

length of the basic cycle for perfect twisted pairs, and thus, increases the electromagnetic coupling between pairs. Equivalently, the pair-center variation increases FEXT to levels that are consistent with those measured in practice. However, pair-center variation alone is not enough to explain the measured NEXT, which necessitates another type of variation, called "twist rate nonuniformity variation."

b) Type II Imperfection in Twisted Pair Cables: Twist Rate Nonuniformity Variations: NEXT is proportional to the constructive reflection when the electromagnetic wave travels along a cable. For a twisted pair cable system with a periodic nature of cable geometry, the effective averaging over a basic period of the twisting causes a uniform appearance of **R**, **L**, **C**, and **G** matrices. Accordingly, the matrix characteristic impedance is uniform. This implies that although there can be minor reflections of electromagnetic waves inside a section of the cable corresponding to one period, there is not much reflection between such periods. In a real cable, uniformity of the cable is not guaranteed. Consequently, larger section-to-section reflections are often created, and lead to the high NEXT levels that are usually observed in measurements. There are a few possible reasons for this "uniformity break": the first reason is the existence of the neighboring pairs. However, simulation results suggest that neighboring pairs do not induce enough reflection. A more likely reason is the twist-rate nonuniformity. The twist rate is defined as the number of twists per unit meter of the pair. This paper uses the following approximation to describe the twist-rate nonuniformity. To model the twist-rate nonuniformity, a twist-rate distribution function is defined. Let $P_{\text{tr}}(\text{tr})$ be the actual probabilistic distribution of the twist rate tr of the real cable and $P'_{\text{tr}}(\text{tr})$ be the ideal probabilistic distribution of the twist rate. The ideal twist-rate distribution is a delta function, $P'_{\text{tr}}(\text{tr}) = \delta(\text{tr} - \overline{\text{tr}})$, where $\overline{\text{tr}}$ is an expected twisted rate for the cable. In a real cable, the twist rate has a nondelta distribution function centered at the expected twist rate. Uniform and Rayleigh distributions for the twist rate are used in simulations to compare with measurement. For the uniform distribution, the following distribution for $P_{\text{tr}}(\text{tr})$ can be used:

$$P_{\text{tr}}(\text{tr}) = \frac{1}{2a}, \qquad \text{tr} \in [\overline{\text{tr}} - a, \overline{\text{tr}} + a]. \tag{27}$$

For practical purposes, $a < 0.2 \cdot \overline{\text{tr}}$ can be chosen. For the Rayleigh distribution, $P_{\text{tr}}(\text{tr})$ is given by

$$P_{\text{tr}}(\text{tr}) = \frac{(\text{tr}) \cdot \exp(-(\text{tr})^2/(2 \cdot (\overline{\text{tr}})^2)}{(\overline{\text{tr}})^2} \tag{28}$$

which has the largest value when $\text{tr} = \overline{\text{tr}}$. To simulate practical systems, overly short or long twist rates can be excluded. After selecting the twist-rate distribution function, the simulation software randomly picks twist rates according to the distribution function, and arranges them along the cable until the complete cable length is reached. Partial twists may be needed at the end of the cable if full twists cannot exactly match the targeted cable length.

c) Type III Imperfection in Twisted Pair Cables: Nontwisted Cable Head or Tail: In real cables, nontwisted tail and head sections may occur at connection points (ends of the cable). Even though the length of the cable tail or head section might only be a few centimeters (a very short length compared to a full-cable length), simulations show that such short nontwisted sections may significantly affect the overall crosstalk level for the whole cable. This is because crosstalk from these nontwisting tail and head sections do not experience any cancellation.

III. Channel Characteristics and Numerical Examples

Based on the preceding circuit theory and cable geometry descriptions, the binder MIMO model can be used to calculate channel transfer functions for a binder or cable from basic system parameters. This section contains results for a few numerical examples and discusses general qualitative characteristics of these models of binder channels. These results are also compared with analytical predictions and measured data. The main purpose of these examples is to verify the model. Since measured data are typically available only for differential excitations, this section focuses on examining the simulation results for differential excitation.

Due to their relative simplicity, crosstalk properties for "single quads" are presented first. Here, crosstalk is shown to be completely cancelled under normal differential excitation. The crosstalk properties for twisted pair cables are then presented with a focus on the effect of cable imperfections. The data show that crosstalk is almost entirely cancelled for an ideal twisted pair cable, but in a real cable, the pair-center variation and the twist-rate variation can greatly affect the crosstalk level. The simulations also show that cable imperfections have a substantial impact on crosstalk, yet have a relatively small impact on the direct transfer function for a twisted pair. Results on how crosstalk depends on cable length will then follow. Simulation results are shown to match well with measured data.

A. Crosstalk for Both Perfect and Imperfect Single Quads

For a perfect basic "single quad," the centers of four wires form a square. The distances between the four wires are denoted as D-D-D-D, where D is the diameter of a wire. For the cable, normal differential excitation is used to excite a pair of diagonal wires, and crosstalk is measured over the other pair of diagonal wires; split-pair differential excitation excites two wires on the same side of a quad, and crosstalk is measured over the other two wires. It can be shown analytically that crosstalk under normal differential excitation is completely cancelled and the cancellation is caused by the perfect geometric symmetry of quad cables. If the symmetry is broken, the crosstalk cancellation mechanism of the diagonally excited quad is degraded. Fig. 4 shows the crosstalk for a quad where the centers of four wires are slightly deviated from a perfect square. The distances of four wires are D-$1.02D$-D-$1.02D$ (2% deviation from a square). Even with such small asymmetry, significant crosstalk under the normal differential excitation is clearly observed. More simulations show that for many practical cables, 2% deviation from a square works as a good approximation to compute crosstalk levels that match measurements.

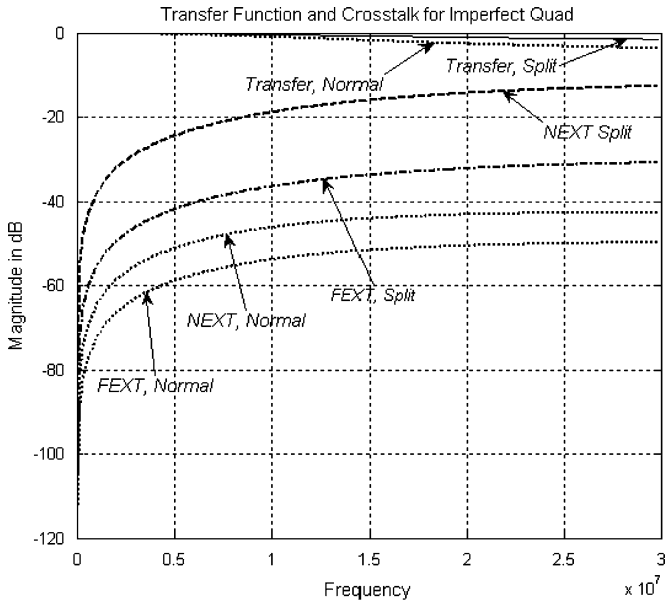

Fig. 4. Crosstalk for 2 m imperfect quad cable.

B. Effects of Cable Imperfection on Crosstalk for Twisted Pair Cables

Fig. 5 shows the effect of cable imperfections on FEXT and NEXT, as well as upon the direct transfer functions between two twisted pairs under normal differential excitation. Here, the normal differential excitation is referred to as exciting two wires in the same twisted pair, and crosstalk is measured for another twisted pair. The length of the cable is 274 m, and the type of the cable is 24 American wire gauge (AWG). The twist rate for one pair is 4.0 in ($\approx$10.1 cm), and for another pair, it is 6.2 in ($\approx$15.7 cm). A parallel layout is used for the simulation, and the expected distance between pair centers is 1.7 mm. The figure shows results for four different scenarios: perfect twisting, with type III imperfection only (untwisted cable head and tail), with types III and I imperfection (pair center variation), and with types III, I, and II imperfection (twist rate variation). Parameters used in describing imperfections are 10% random pair-center variation, 3 cm untwisted cable head and tail, and uniform twist-rate distribution, where $P_{\text{tr}}(\text{tr}) = 1/2a,\ \text{tr} \in [\overline{\text{tr}} - a, \overline{\text{tr}} + a]$,$a = 0.15 \cdot \overline{\text{tr}}$. A few outstanding characteristics can be observed in this figure. First, without cable imperfection, both FEXT and NEXT are very small, which illustrates that the crosstalk is mostly cancelled for perfect twisted pairs, but this cancellation is not as complete as for the earlier example of the "quad" cables. This conclusion is analytically proved in [15]. Second, imperfections have a big impact on FEXT and NEXT levels; in particular, the twist-rate variation causes the NEXT to exhibit irregular patterns of notches and peaks over frequency. Third, the direct-pair transfer function is not significantly affected by imperfections. Even though these simulation results are obtained for the specific parameters used in this example, the general trends hold for other parameters. In general, simulation results suggest that for a twisted pair cable system, cable imperfections have great impact on crosstalk under normal differential excitation, but small impact on crosstalk under split-pair differential excitation [15]. Here, split-pair differential excitation is defined as follows: for two twisted pairs, a source is excited between two wires in different twisted pairs, and crosstalk is measured over the remaining two wires. Additionally, if nondifferential excitation is used, such as the source and load impedances being matrix matched to the cable binder, cable imperfections are shown to have small impact on the crosstalk and direct-line transfer functions [15].

C. Crosstalks versus Cable Length

This section presents how crosstalk depends on cable length, which had been reported as experimental and theoretical results in literature [23]. This section shows that the model and simulation presented in this paper can also reveal a similar effect, further proving the usefulness of the model. Fig. 6(a) shows an example of how NEXT and FEXT, as well as the direct pair transfer function, vary under the normal differential excitation when the cable length changes. This particular cable contains two pairs. The twist rates are 2.0 in ($\approx$0.051 m) and 3.9 in ($\approx$0.099 m) for each of the two twisted pairs. The figure plots the average direct transfer function, NEXT, and FEXT over the frequency range of 0–20 MHz. In Fig. 6(a), the cable length changes from 274 to 274.2 m. As expected, the direct transfer function remains almost constant when the cable length has such small variations. However, both NEXT and FEXT are very sensitive to the cable length variations, even though the variations are smaller than the twist rates. The effect, named here as the "large crosstalk variations due to partial twist," has been observed in measurements [9], [17] and theoretically analyzed in [9] and [15]. The large crosstalk variations due to partial twist effect could have a considerable impact on the S/N for twisted pairs under the usual differential excitation when FEXT dominates other noises. Furthermore, simulation results suggest that this effect happens only under the normal differential excitation but not under split-pair differential excitation. Additionally, simulations show that a nontwisted cable head or tail can cause a similar effect. Fig. 6(b) shows a related but different effect. It shows how the direct-line transfer function and crosstalk vary with large cable length changes. The simulation uses same parameters as in Fig. 6(a) except that the cable length changes from 20 to 1200 m. As can be seen from the figure, the direct transfer function monotonically decreases as the cable length increases, but the crosstalk does not decrease monotonically. The nonmonotonic decrease of crosstalk is not at all caused by the partial-twist effect. This is because the nonmonotonic dependence on cable length is still observed even if the cable length is carefully chosen such that the partial twist is completely removed. Consequently, the S/N can vary by a few decibels when the cable length increases. Therefore, a receiver closer to the source might have worse S/N than a receiver at a greater distance, with the usual differential excitation.

D. Simulation Vs. Measured Data

Fig. 7(a) shows the measured values of the direct transfer function of a pair, NEXT, and FEXT between two pairs in

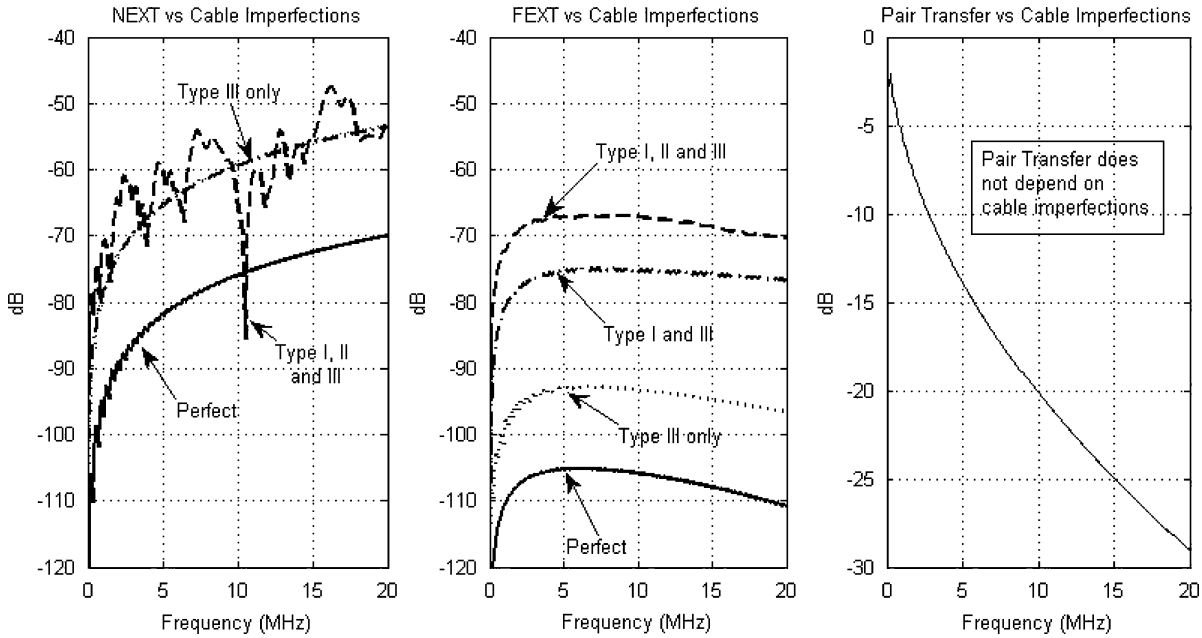

Fig. 5. Effect of cable imperfection on crosstalk under normal differential excitation: 274 m, 24 AWG.

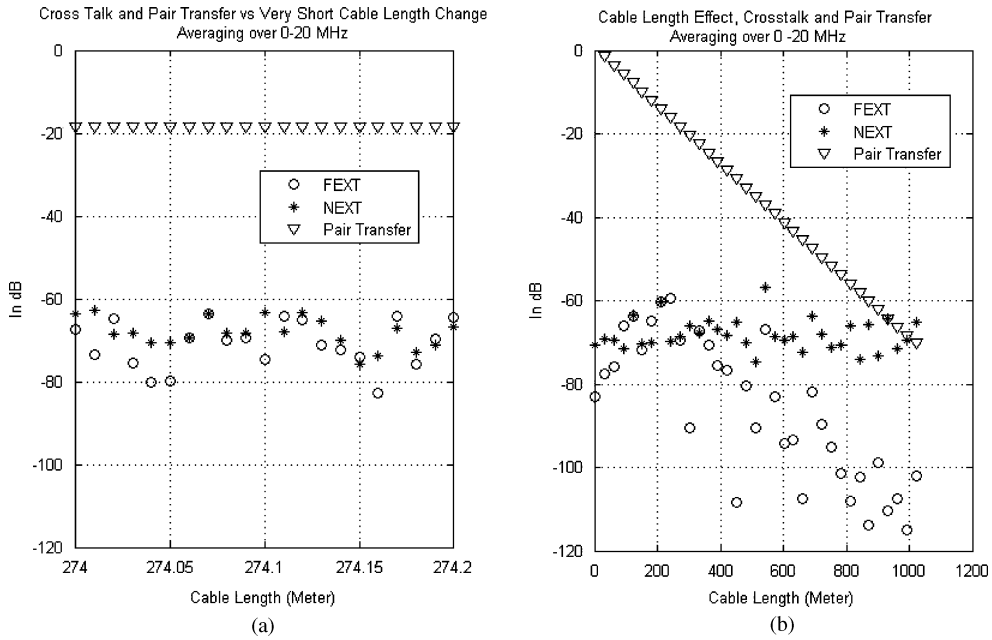

Fig. 6. Crosstalk as a function of partial twist and cable length.

a real cable system. The cable consists of 25 twisted pairs (24 AWG) of 274 m length. The selected pairs are surrounded by neighboring pairs. The data were measured using a network analyzer (Agilent 4395A); 50–100 Ω baluns were used when needed. Fig. 7(b) shows the simulation results with 10% random pair-center variation and uniform twist-rate distribution, $P_{\text{tr}}(\text{tr}) = 1/2a,\ \text{tr} \in [\overline{\text{tr}} - a, \overline{\text{tr}} + a]$, where $a = 0.15 \cdot \overline{\text{tr}}$, are used. The simulation assumed two adjacent 24 AWG pairs, each of length 274 m. The two pairs are initially parallel. These two pairs are isolated in the air. A 100 Ω source and load impedances are used in each pair. Physical constants μ, ε_r, and σ (permittivity, permeability, and conductivity, respectively) of the dielectric filling material of cables and resistance of cable are extracted [15]. They are all frequency dependent. The simulation results depend on the random-number generator (each random output of which, of course, represents a specific cable). The figure shows the result for one specific random number generator, which matches the measured data well suggesting that this particular random number is a good match to the specific cable. Note that the simulated FEXT is still "smoother" than

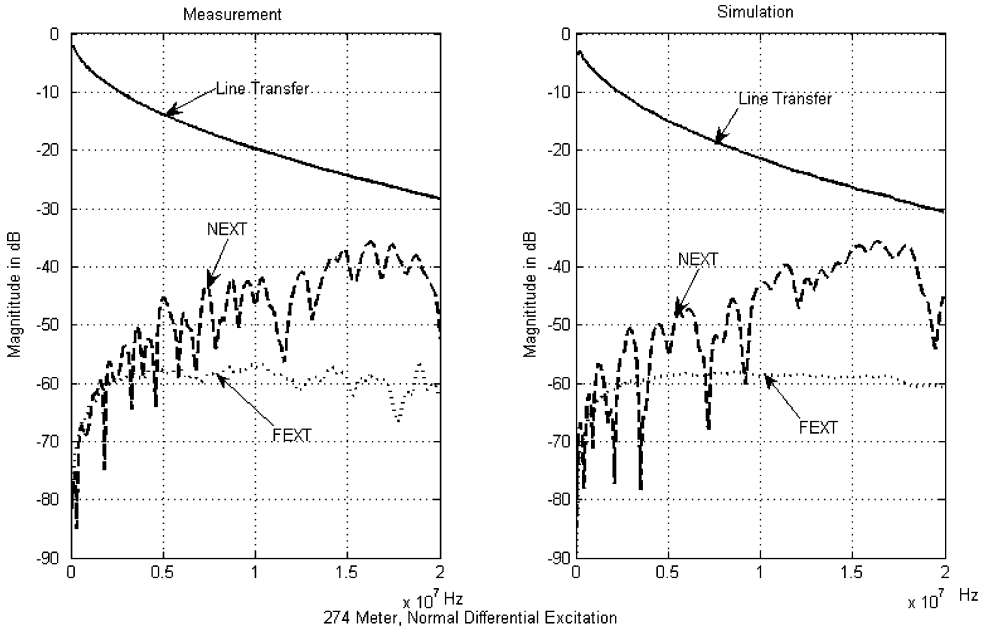

Fig. 7. Simulation versus measurement.

the measured data. The "roughness" of the measured FEXT can be caused by neighboring pairs and other cable imperfections, which were not included in the simulation.

The numerical results generated by the simulations in this paper depend on specific sets of cable parameters, and in some cases, the random number generators. These results should be considered as more exploratory than definitive. In addition to the aforementioned examples, the binder MIMO model has been used to generate power sum for all crosstalk components in a cable binder, and simulation results have been compared with empirical results [12]. Results for practical achievable data rates using the common-mode MIMO channel are reported in [18]. The complete simulation software suites are available upon request.

IV. Conclusion

In this paper, a binder MIMO channel model is proposed to characterize the physical channels including all transfer functions and crosstalk couplings of multiwire communication systems. The model is flexible in that it can accommodate various kinds of practical cables with different cable geometries, source–load configurations, and different types of cable imperfections. The model can be used not only to calculate NEXT and FEXT when a cable is used under (traditional) differential excitations, but also to calculate a MIMO channel matrix **H** when the system uses MIMO transmission methods. Once the channel matrix H is revealed, the achievable data rate of multiwire communication systems can be calculated. The model builds a relationship between the channel matrix **H** and the actual physical parameters such as source–load configurations, cable types, and geometry parameters; therefore, it can relate the achievable data rate with these parameters and provide helpful insights in real system designs. The proposed model does not include the effect of cable shielding or bridge taps, which are left for future work.

Acknowledgment

The authors wish to thank the reviewers and the associate editor for providing many constructive comments and suggestions, which have improved the quality of this paper.

References

[1] T. Starr, M. Sorbara, J. M. Cioffi, and P. J. Silverman, *DSL Advances*. Englewood Cliffs, NJ: Prentice Hall, 2003.

[2] G. Ginis and J. M. Cioffi, "Vectored transmission for digital subscriber line systems," *IEEE J. Sel. Areas Commun.*, vol. 20, no. 5, pp. 1085–1104, Jun. 2002.

[3] T. Starr, J. M. Cioffi, and P. J. Silverman, *Understanding Digital Subscriber Line Technology*. Englewood Cliffs, NJ: Prentice Hall, 1999.

[4] C. R. Paul, *Analysis of Multiconductor Transmission lines*. Hoboken, NJ: Wiley, 1994.

[5] S. O. Rice, "Steady state solutions of transmission line equations," *Bell Syst. Tech. J.*, vol. 20, pp. 131–178, Apr. 1941.

[6] S. Jagannathan, V. Pourahmad, K. Seong, J. M. Cioffi, M. Ouzzif, and R. Tarafi, "Common-mode data transmission using the binder sheath in digital subscriber lines," *IEEE Trans. Commun.*, submitted.

[7] C. R. Paul and J. W. McKnight, "Prediction of crosstalk involving twisted pairs of wires—Part I: A transmission-line model for twisted-wire pairs," *IEEE Trans. Electromagn. Compat.*, vol. 21, no. 2, pp. 92–105, May 1979.

[8] C. R. Paul, *Introduction to Electromagnetic Compatibility*. Hoboken, NJ: Wiley, 1992, ch. 10.

[9] C. R. Paul and M. B. Jolly, "Sensitivity of crosstalk in twisted pair circuits to line twist," *IEEE Trans. Electromagn. Compat.*, vol. 24, no. 3, pp. 359–364, Aug. 1982.

[10] D. Bellan, S. A. Pignari, and G. Spadacini, "Characterisation of crosstalk in terms of mean value and standard deviation," *Inst. Electr. Eng. Proc. Sci., Meas. Technol.*, vol. 150, no. 6, pp. 289–295, Nov. 2003.

[11] C. Valenti, "NEXT and FEXT models for twisted pair north American loop plant," *IEEE J. Sel. Areas Commun.*, vol. 20, no. 5, pp. 893–900, Jun. 2002.

[12] J. Cioffi, B. Lee, M. Mohseni, M. H. Brady, K. Seong, and Y. Kim, "Evolving channel modeling text for section 5.1 of DSM report," *ANSI Contribution T1E1.4/2003-033R2*, Aug. 2003.

[13] J. Lee, "Modeling and characterization of copper access systems," Ph.D. dissertation, Dept. Electr. Eng., Stanford Univ., Stanford, CA, 2002.
[14] J. A. B. Faria and M. V. G. das Neves, "Analysis of the helical twisted-wire pair running above ground: Transfer function evaluation," *IEEE Trans. Electromagn. Compat.*, vol. 45, no. 2, pp. 449–453, May 2003.
[15] B. Lee, "Binder MIMO channel" Ph.D. dissertation, Dept. Electr. Eng., Stanford Univ., Stanford, CA, 2004.
[16] M. B. Jolly and C. R. Paul, *Basic EMC Technology Advancement for C3 Systems—Crosstalk in Twisted-Wire Circuits*, RADC-TR-82-286, New York: Rome Air Development Center, Griffiss Air Force Base, vol. IV C, 1982.
[17] D. Joffe, "End effects on capacitance and inductance measurements in paired cable," *ANSI Contribution T1E1.4/2002-238*, Nov. 2002.
[18] B. Lee, J. Cioffi, S. Jagannathan, and M. Mohseni, "Gigabit DSL," *IEEE Trans. Commun.*, to be published.
[19] N. Holte, "Calculation of crosstalk in balanced pair cables by means of simulation," presented at the Int. Wire Cable Symp., Cherry Hill, NJ, Nov. 1977.
[20] L. M. Wedepohl, "Application of matrix methods to the solution of travelling-wave phenomena in polyphase systems," *Proc. Inst. Electr. Eng.*, vol. 110, no. 12, pp. 2200–2212, Dec. 1963.
[21] H. W. Friesen, "Relating the twist detection measurements of twisted pairs to their crosstalk performance," in *Proc. Int. Wire Cable Symp.*, Cherry Hill, NJ, Nov. 1975, pp. 150–157.
[22] H. W. Friesen, "Experimental verification of near end crosstalk equation for balanced telephone cable pairs," in *Proc. Nat. Telecommun. Conf.*, Nov. 1973, pp. 8C-1–8C-11.
[23] T. A. Lenahan, "The theory of uniform cables—Part I: Calculation of propagation parameters. Part II: Calculation of charge components," *Bell Syst. Tech. J.*, vol. 56, pp. 597–624, Apr. 1977.
[24] N. Holte, "A crosstalk model for cross-stranded cables," presented at the Int. Wire Cable Symp., Cherry Hill, NJ, Nov. 1982.
[25] H. Cravis and T. V. Crater, "Engineering of T1 carrier system repeated lines," *Bell Syst. Tech. J.*, vol. 42, pp. 431–486, Mar. 1963.
[26] J. Gibbs and R. Addie, "The covariance of near end crosstalk and its application to PCM system engineering in multipair cable," *IEEE Trans. Commun.*, vol. 27, no. 2, pp. 469–477, Feb. 1979.

Bin Lee received the B.S. degree in physics from Nankai University, Tianjin, China, in 1990, the M.S. degree in physics from Virginia Tech, Blacksburg, in 1993, and the Ph.D. degree in electrical engineering from Stanford University, Stanford, CA, in 2004.

He was with companies like Analog Devices, Ciena, Inc., and ASSIA, Inc. He is currently an individual Consultant. His current research interests include communications systems, networking, and Internet applications.

John M. Cioffi (S'77–M'78–SM'90–F'96) received his B.S.E.E. degree in electrical engineering from the University of Illinois at Urbana-Champaigne, Urbana, in 1978 and the Ph.D. degree in electrical engineering from Stanford University, Stanford, CA, in 1984.

He was with Bell Laboratories, Murray Hill, NJ, from 1978 to 1984 and with IBM Research from 1984 to 1986. He joined Stanford University as a Professor in 1986, where he is currently the Hitachi America Professor of Electrical Engineering. He founded Amati Com. Corporation in 1991 (purchased by TI in 1997) and was its Officer/Director from 1991 to 1997. He is on the Board of Directors of ASSIA (Chair), Afond, Teranetics, and ClariPhy. He is on the Advisory Boards of Portview Ventures, Wavion, MySource, and Amicus. His research interests include the area of high-performance digital transmission.

Prof. Cioffi is a member of the National Academy of Engineering and a Marconi Fellow. He received the IEEE Kobayashi Medal in 2001, the IEEE Millennium Medal in 2000, the IEEE Fellow in 1996, the IEE J.J. Tomson Medal in 2000, the 1999 University of Illinois Outstanding Alumnus, the 1991 IEEE Communications Magazine Best Paper, the 1995 ANSI T1 Outstanding Achievement Award, the NSF Presidential Investigator from 1987 to 1992, and the ISSLS 2004 Outstanding Paper Award. He has authored over 250 papers published in several journals and conference proceedings. He is the holder of over 80 patents.

Sumanth Jagannathan (S'01) received the B.Tech. degree in electrical engineering from the Indian Institute of Technology (IIT), Chennai, India, in 2003, and the M.S. degree in electrical engineering in 2005 from Stanford University, Stanford, CA, where he is currently working toward the Ph.D. degree in electrical engineering.

His current research interests include communication theory, multiuser information theory, and their applications to wireline and wireless communications including digital subscriber line (DSL), orthogonal frequency-division multiplexing (OFDM), and multiple-antenna systems.

Kibeom Seong (S'05) received the B.S. and M.S. degrees in electrical engineering from Seoul National University, Seoul, Korea, in 1997 and 1999, respectively. He is currently working toward the Ph.D. degree in electrical engineering at Stanford University, Stanford, CA.

From 1999 to 2002, he was a Faculty Member in the Department of Electrical Engineering, Korea Military Academy, Seoul. He is currently with Qualcomm, Inc., San Diego, CA. His current research interests include communication theory, multiuser information theory, and dynamic resource management in wireless and wireline communication systems.

Youngjae Kim (S'02) received the B.S.E.E. degree in 1999 from Seoul National University, Seoul, Korea, in 1999, and the M.S.E.E. and Ph.D. degrees from Stanford University, Stanford, CA, in 2003 and 2007, respectively, all in electrical engineering.

He worked as a Student Manager at SBC (AT&T) Laboratories, where he was involved in dynamic spectrum management (DSM) simulations. During the summer of 2004 and 2005, he was a Graduate Intern at Intel Corporation, where he simulated closed-loop schemes for multiantenna wireless LAN systems. Since August 2006, he has been a Systems Engineer with Texas Instruments, Inc., Dallas. His current research interests include signal processing and algorithm development for wireless and wireline digital communication systems.

Mehdi Mohseni (S'02) received the B.S. degree from Sharif University of Technology, Tehran, Iran, in 2001, and the M.S. and Ph.D. degrees from Stanford University, Stanford, CA, in 2003 and 2006, respectively, all in electrical engineering.

He is currently with ASSIA, Inc., Redwood City, CA. His current research interests include multiuser information theory, convex optimization techniques, and their application to wireless and broadband communications.

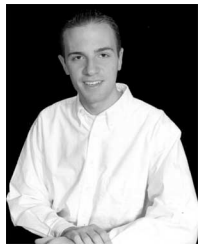

Mark H. Brady received the B.S.E.E. degree from the University of Illinois at Urbana-Champaign, Urbana-Champaign, in 2001, and the Ph.D. degree from Stanford University, Stanford, CA, in 2006, both in electrical engineering.

He is currently a Technology Architect with ASSIA, Inc., Redwood City, CA. His current research interests include digital subscriber line (DSL) systems, optimization theory, and information theory.